UMEÅ UNIVERSITY MEDICAL DISSERTATIONS
New series No. 1009

Adaptive signal processing of surface electromyogram signals

Nils Östlund

Department of Radiation Sciences, Umeå University, Sweden
Department of Biomedical Engineering and Informatics,
University Hospital, Umeå, Sweden
Umeå 2006

ISSN 0346-6612
ISBN 91-7264-033-2

Printed by Print & Media,
Umeå University, Sweden, 2006

"The important thing in science is not so much to obtain new facts as to discover new ways of thinking about them"

William Bragg (1862-1942)

Abstract

Electromyography is the study of muscle function through the electrical signals from the muscles. In surface electromyography the electrical signal is detected on the skin. The signal arises from ion exchanges across the muscle fibres' membranes. The ion exchange in a motor unit, which is the smallest unit of excitation, produces a waveform that is called an action potential (AP). When a sustained contraction is performed the motor units involved in the contraction will repeatedly produce APs, which result in AP trains. A surface electromyogram (EMG) signal consists of the superposition of many AP trains generated by a large number of active motor units. The aim of this dissertation was to introduce and evaluate new methods for analysis of surface EMG signals.

An important aspect is to consider where to place the electrodes during the recording so that the electrodes are not located over the zone where the neuromuscular junctions are located. A method that could estimate the location of this zone was presented in one study.

The mean frequency of the EMG signal is often used to estimate muscle fatigue. For signals with low signal-to-noise ratio it is important to limit the integration intervals in the mean frequency calculations. Therefore, a method that improved the maximum frequency estimation was introduced and evaluated in comparison with existing methods.

The main methodological work in this dissertation was concentrated on finding single motor unit AP trains from EMG signals recorded with several channels. In two studies single motor unit AP trains were enhanced by using filters that maximised the kurtosis of the output. The first of these studies used a spatial filter, and in the second study the technique was expanded to include filtration in time. The introduction of time filtration resulted in improved performance, and when the method was evaluated in comparison with other methods that use spatial and/or temporal filtration, it gave the best performance among them. In the last study of this dissertation this technique was used to compare AP firing rates and conduction velocities in fibromyalgia patients as compared with a control group of healthy subjects.

In conclusion, this dissertation has resulted in new methods that improve the analysis of EMG signals, and as a consequence the methods can simplify physiological research projects.

Contents

Original papers 9

Abbreviations 10

Introduction 11

- Basic anatomy and physiology 11
- Electromyography 12
  - Signal acquisition 13
  - Noise sources 14
  - Electrode configurations 14
  - Models 14
- Statistics 16
  - Moments and cumulants 16
  - Sensitivity, specificity and predictivity 17
- Power spectral estimation 19
  - Short-time Fourier transform 19
  - Wavelets 20
  - Continuous wavelet transform 20
  - Bilinear distributions 22
  - Spectral moments 22
- Component analysis 23
  - Principal Component analysis 24
  - Independent Component analysis 24
- Electromyography techniques 24
- Aims 25
  - Specific aims 25

Materials and methods 27

- Simulations 27
- Experimental procedures 27
- Subjects 27
- Location of innervation zone 28
- Estimation of mean frequency 28
- Adaptive filtration 30

Spatial and spatio-temporal filters 32

Results 35

Location of innervation zone 35
Mean frequency estimation 36
Adaptive filtration 38

Discussion 41

Location of innervation zone 41
Mean frequency estimation 42
Adaptive filtration 42
Future methods and applications 43
Conclusions 44

Acknowledgements 45

References 47

Appendix 51

Introduction to the JADE algorithm 51

Original papers

This thesis is based on the following papers[†], which are referred to by their Roman numerals in the text.

I. ÖSTLUND N., GERDLE B., AND KARLSSON J. S., "Location of innervation zone determined from multichannel surface EMG signals using an optical flow technique", *Manuscript*

II. ÖSTLUND N., YU J., AND KARLSSON J. S., (2004): "Improved maximum frequency estimation with application to instantaneous mean frequency estimation of surface electromyography", *IEEE Trans. Biomed. Eng.*, **51**, pp. 1541-1546

III. ÖSTLUND N., YU J., ROELEVELD K., AND KARLSSON J. S., (2004): "Adaptive spatial filtering of multichannel surface electromyogram signals", *Med. Biol. Eng. Comput.*, **42**, pp. 825-831

IV. ÖSTLUND N., YU J., AND KARLSSON J. S., "Adaptive spatio-temporal filtering of multichannel surface EMG signals", *Med. Biol. Eng. Comput.*, **in press**

V. GERDLE B., ÖSTLUND N., GRÖNLUND C., ROELEVELD K., AND KARLSSON J. S., "Motor unit firing rate and conduction velocity of the trapezius muscle in fibromyalgia patients and healthy controls", *Manuscript*

[†] Papers II, III, and IV are reprinted with permission from the publishers.

Abbreviations

AP	action potential
BSS	blind source separation
CV	conduction velocity
CWT	continuous wavelet transform
ECG	electrocardiogram
EMG	electromyogram
FN	false negative
FP	false positive
IB2	inverse binomial of order two
ICA	independent component analysis
IMNF	instantaneous mean frequency
IR	inverse rectangle
IZ	innervation zone
JADE	joint approximate diagonalisation of eigenmatrices
LDD	longitudinal double differential
LSD	longitudinal single differential
MKF	maximum kurtosis filter
MNF	mean frequency
MU	motor unit
MUAP	motor unit action potential
NDD	normal double differential
NMJ	neuromuscular junction
PCA	principal component analysis
PSD	power spectral density
RBTM	running block threshold method
RMS	root-mean-square
ROC	receiver operating characteristic
TCM	threshold crossing method
TFR	time-frequency representation
TN	True negative
TP	True positve
SNR	signal-to-noise ratio
STFT	short-time Fourier transform
WLPD	weighted low-pass differential

Introduction

Electromyography is the study of muscle function through the electrical signals from the muscles. In surface electromyography the electrical signal, the electromyogram (EMG[†]) signal, is detected on the skin. The signal arises from ion exchanges across the muscle fibres' membranes. The EMG signal, when recorded with electrodes on the skin, is a very complex signal due to the summation of signals from many muscle fibres. Surface electromyography is mainly used in the fields of ergonomics, biomechanics, sport sciences, and rehabilitation (Hermens *et al.*, 1997; Merletti and Parker, 2004), where it is often used to estimate muscle force, timing of different muscles, or muscle fatigue.

Surface EMG recordings are unfortunately influenced by many parameters that are of no direct interest, for example the electrode-skin impedance. It would be desirable that the methods, which are used for the analysis of the EMG signals, could adapt to the recording situation and make the measurements less dependent on these parameters. This dissertation is a step in that direction. In signal processing literature the term *adaptive filter* often refers to a technique in which the filter coefficients are updated with a correction term that has been estimated from an error signal. In this thesis the word adaptive has a wider meaning and refers to the fact that the methods are adapted to the recorded data.

Basic anatomy and physiology

The primary function of muscles is to change chemical energy into mechanical energy. When the word muscle is used in this thesis it refers to a skeletal muscle. However, there are also two other types of muscles: cardiac and smooth muscles.

The skeletal muscle cells are often referred to as muscle fibres. The muscle fibres contain several myofibrils, which can change their lengths by sliding filaments (Tortora and Grabowski, 2003). A muscle is able to

[†] In this thesis EMG refers to surface EMG, unless otherwise specified.

produce movement due to the myofibrils' ability to change their length. A muscle fibre is activated when the neurotransmitter acetylcholine is released in the synapse between the neuron and the muscle fibre, called the neuromuscular junction (NMJ). The release of acetylcholine results in a flow of ions (most importantly Na^{+}) through the cell membrane (sarcolemma). The change of potential over the sarcolemma is called an action potential (AP). The NMJ is often located in the middle of the muscle fibre so the AP is spread in both directions along the muscle fibre. The speed of the propagation of the AP is called conduction velocity (CV). When the AP propagates it results in the release of Ca^{2+} from the sarcoplasmic reticulum. The Ca^{2+}, in turn, triggers the sliding of the filaments in the myofibrils.

Somatic motor neurons are usually connected to many muscle fibres, and each neuron together with the muscle fibres it innervates is called a motor unit (MU). An MU normally consists of 10 to 3000 muscle fibres (Tortora and Grabowski, 2003) that contract at the same time. Muscles that require fine precision have few muscle fibres per MU and muscles where the force is more important have many muscle fibres per MU.

An AP results in a twitch contraction that lasts about 20 to 200 milliseconds. In order to produce a more constant force the MU is repeatedly activated resulting in an AP train. The timing of the repeated APs seems to be random. In this way it is assured that different MUs are not activated precisely at the same time. The stochastic behaviour is therefore a way to obtain a smoother movement.

Electromyography

A definition of electromyography that is often used today is the introduction sentence from *Muscles Alive* by Basmajian and DeLuca (1985):

> "Electromyography is the study of muscle function through the inquiry of the electrical signal the muscles emanate".

This definition will be used in this thesis and the recorded electrical signal is referred to as the EMG signal. In 1792 Luiggi Galvani discovered that muscles and electricity have a connection, but in the years to come research on muscle electricity was rare. Gasser and Erlanger were the first to visualise APs for which, together with the interpretation of the AP, they were rewarded with the Nobel Prize in 1944 (Basmajian and DeLuca, 1985).

The introduction of the concentric needle electrode by Adrian and Bronk (1929) was the start of the development of the clinical aspects of

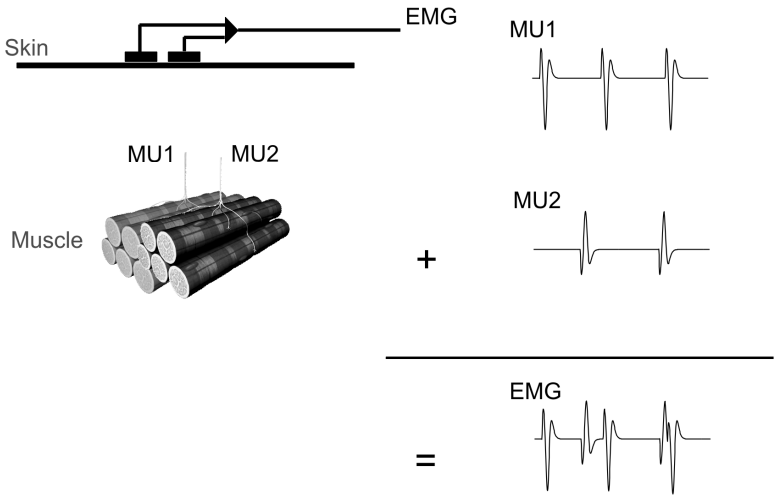

Figure 1. Schematic description showing the EMG signal as a summation of motor unit action potential trains. For simplicity the muscle consists of very few muscle fibres and only two MUs. The image of the muscle fibres are courtesy of 3DScience.com.

electromyography. The needle EMG is still by far the most common technique for diagnostic applications.

Signal acquisition

In surface EMG, the signal is recorded with electrodes on the surface of the skin. The tissue located between the electrodes and the source of the signal will act as a volume conductor. Currents are conducted through the tissue, but due to the properties of the biological tissue, the amplitude of the signal will be reduced, especially for higher frequencies. The tissue is therefore acting as a low-pass filter (Lindström and Magnusson, 1977). Nevertheless, the surface-recorded potential from an MU is still called an AP even if it is heavily filtered. However, due to the fact that the surface electrodes record signals from a large part of the muscle, the surface EMG is an interference signal consisting of a large number of AP trains (see Fig. 1).

Noise sources

Unfortunately, the recorded EMG signal does not only consist of a summation of APs from active MUs, but also of noise that derives from different sources. Stretching and relaxing the skin produce motion artefacts (de Talhouet and Webster, 1996). The motion artefacts are typically low-frequency noise with its main energy below 20 Hz. Other sources of noise are interference from the electrode-skin interface, power-line interference, cross talk (muscle activity from other muscles), electrical activity from the heart, amplifier noise, and external sources (Clancy *et al.*, 2002; Huigen *et al.*, 2002).

Electrode configurations

In surface EMG a recording of a linear combination of signals from different electrodes is often used. By far the most common linear combination is a bipolar configuration (differential recording). The linear combinations can be seen as spatial filters defined by their filter masks showing the weights and their spatial locations. For example, the laplace or normal double differential (NDD) filter can be defined with the following filter mask:

$$A^{NDD} = \begin{bmatrix} 0 & -1 & 0 \\ -1 & 4 & -1 \\ 0 & -1 & 0 \end{bmatrix}. \tag{1}$$

The spatial filters are almost always designed as a spatial high-pass filter in order to limit the electrodes' uptake area, reduce noise, and enhance single APs (see Fig. 2).

Models

EMG models are well suited and often indispensable for testing and comparing different methods (Merletti and Parker, 2004). EMG recorded with ordinary bipolar electrodes resembles coloured noise and is often modelled as such. A popular shape of the power spectral density (PSD) is the shape proposed by Shwedyk *et al.* (1977). Stulen and DeLuca (1981) parameterised that shape with the following PSD:

$$PSD(f) = \frac{c f_2^4 f^2}{\left(f^2 + f_1^2\right)\left(f^2 + f_2^2\right)^2}, \tag{2}$$

where f_1 and f_2 are the cut-off frequencies.

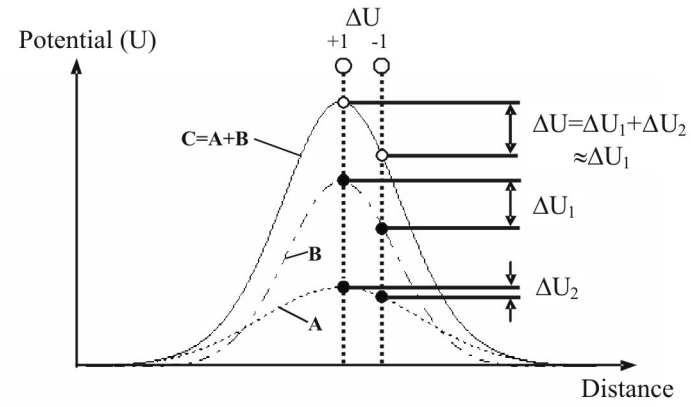

Figure 2. An MU located close to the skin surface generates a spatially steep potential (B) and a deeper MU generates a spatial potential that is more flat (A). Both potentials contribute to the total potential (C), but the potential recorded as the difference between two closely located electrodes (ΔU) is almost only affected by the MU that is closer to the skin. This figure is a modified figure from Grönlund (2005) with permission.

When methods that enhance single APs are to be evaluated, more advanced models are needed. Four models (RRDsim, Anvolcon, SiMyo, and EMG-Sim) are freely available from the project "Surface EMG for Non-Invasive Assessment of Muscles" (Hermens *et al.*, 1999). These models allow the EMG signals to be simulated as the superposition of single MU action potentials (MUAPs).

Another model, introduced by Farina and Merletti (2001b), describes the volume conductor as a transfer function. Farina and Merletti suggested using the mathematical model of the source as described by Rosenfalck (1969). The source signal is assumed to travel along a muscle fibre. The source signal is then filtered using a transfer function consisting of different parts that mimic the influence of the muscle, the fat layer, the skin layer (see equation (3)), and the recording electrode (equation not shown).

$$H_{vc}\left(k_x,k_z\right)=\frac{2}{\sigma_{2a}}e^{-k_{ya}|y_0|}\left\{\left(1+R_c\right)\cosh\left[k_y\left(h_1+d\right)\right]\alpha\left(k_y\left(h_1+d\right)\right)+\left(1-R_c\right)\cosh\left[k_y\left(h_1-d\right)\right]\alpha\left(k_y\left(h_1-d\right)\right)\right\}^{-1}, \tag{3}$$

where

d = thickness of the skin layer

h_1 = thickness of the fat layer

y_0 = depth of the source in the muscle

σ_{2a} = the conductivity across the muscle fibres

R_a = the conductivity along the muscle fibres divided by the conductivity across the muscle fibres

R_c = the conductivity of the skin layer divided by the conductivity of the fat layer

R_m = the conductivity of the fat layer divided by the conductivity across the muscle fibres

k_x and k_z are the spatial angular frequencies

$k_y=\sqrt{k_x^{\,2}+k_z^{\,2}}$

$k_{ya}=\sqrt{k_x^{\,2}+R_a k_z^{\,2}}$

$\alpha\left(s\right)=k_{ya}+k_y R_m tgh(s).$ (4)

The above equation (4) was incorrectly written in the paper by Farina and Merletti (2001b) and is given correctly here. By summing simulated repeatedly activated source signals, which are located in different parts of the muscle and therefore filtered with different transfer functions, a simulated surface EMG signal can be created. This model simulates the volume conductor as flat layers, but in a later article (Farina *et al.*, 2004) the model was extended to a cylindrical volume conductor.

Statistics

Moments and cumulants

If the random variable X has a density function $f(x)$, then the expectation of the function g(X) is:

$$\mathrm{E}(g(X))=\int_{-\infty}^{\infty}g(x)f(x)dx. \tag{5}$$

In particular

$g(X) = X^r \Rightarrow$ moment of order r

$g(X) = (X - u)^r \Rightarrow$ central moment of order r,
where u is the mean (first moment)

$g(X) = e^{tX} \Rightarrow$ moment-generating function.

The power series representation of the moment-generating function contains the moments of the distribution. The logarithm of the moment-generating function is called the cumulant-generating function and the nth coefficient in the power series of this function is $\kappa_n/n!$, where κ_n is the cumulant of order n. The reason for using cumulants instead of moments is that calculations become simpler. The first three cumulants are identical to the first three central moments. The third cumulant (or central moment) is often expressed in normalised form as $\kappa_3/\kappa_2^{3/2}$ and called skewness. Skewness is used as a measure of asymmetry of the probability distribution. The normalised fourth order central moment and the fourth order normalised cumulant are both called kurtosis. Due to the normalisation, skewness and kurtosis are dimension-free (not depending on the units of measurements). The definition of kurtosis from the central moments is called kurtosis proper and is calculated as μ_4/μ_2^2, where μ_r denotes the rth central moment. The definition from cumulants, called kurtosis excess, is $\kappa_4/\kappa_2^2 = \mu_4/\mu_2^2$-3. As seen in the equation the difference between kurtosis proper and kurtosis excess is only the term -3. For example, the normal distribution has a kurtosis excess of 0 and a kurtosis proper of 3. In this thesis when the word kurtosis is solely used it refers to kurtosis excess. Kurtosis is often used as a measure of the peakedness of a distribution (outlier-prone), but it can also be used to find a bimodal distribution (distribution with two separated peaks) (Darlington, 1970).

Sensitivity, specificity and predictivity

If we have a test with only two possible results (dichotomous test) it is possible to draw a two by two table as seen in Figure 3.

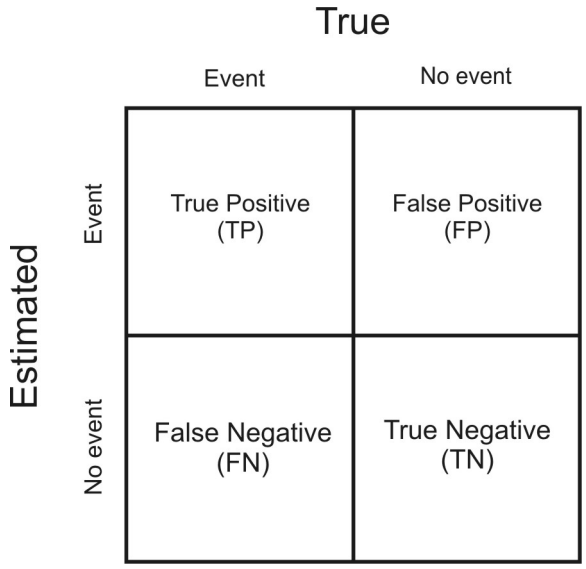

Figure 3. Definition of true positives, false positives, true negatives, and false negatives.

With help from the table in Figure 3, which defines TP, FP, FN, and TN, it is possible to define the sensitivity, which is the percentage of all positive cases we find, as:

$$\text{sensitivity} = TP/(TP+FN).$$

The percentage of all negative cases we find is called specificity and is defined as:

$$\text{specificity} = TN/(TN+FP).$$

To make the list more complete we can also define:

$$\text{positive predictivity} = TP/(TP+FP)$$
$$\text{negative predictivity} = TN/(TN+FN)$$
$$\text{accuracy} = \frac{TP+TN}{TP+TN+FP+FN}.$$

The FP is sometimes referred to as Type I error and the FN as Type II error.

Since it is possible to calculate many different statistics, and they are to some extent dependent on each other, it has been increasingly popular to draw receiver operating characteristic curves (ROCs). The name originates from the application with radio signals. An ROC is drawn as the true positive rate (sensitivity) as a function of false positive rate (1-specificity) and then the area below the curve is often calculated.

The sensitivity and specificity are probably the most common statistics calculated from dichotomous tests. However, for detection algorithms (as those presented in this thesis) it is hard to define true negatives and therefore the specificity can not be calculated. It has been proposed to use the sensitivity along with the positive predictivity for detection algorithms (Farina *et al.*, 2001a).

Power spectral estimation

The Fourier transform uses a combination of complex sinusoids of different frequencies to characterise the frequency content of the signal. Because the sinusoids are localized in frequency but not in time the method can only be applied to stationary signals; that is when the frequency contents do not change with time. For many signals found in real life this property does not hold, which is the case for EMG signals. When there is a requirement for resolution in both time and frequency, a time-frequency representation (TFR) is needed.

Short-time Fourier transform

A way to get the Fourier transform time-dependent is to use a short window on the signal $x(t)$. This is exactly what is done in the short-time Fourier transform (STFT):

$$STFT(f,t) = \int \gamma^*(\tau - t)x(\tau)e^{-j2\pi f\tau}d\tau, \tag{6}$$

where $\gamma(t)$ is the window function and * stands for the complex conjugate. The choice of window function and length determines the time and frequency resolution. There is a trade-off between time and frequency resolution. If there is a need for a better time resolution the frequency resolution will be worse and vice versa. The sampled STFT with a Gaussian window is also known as the Gabor transform and the squared magnitude of the STFT is called spectogram.

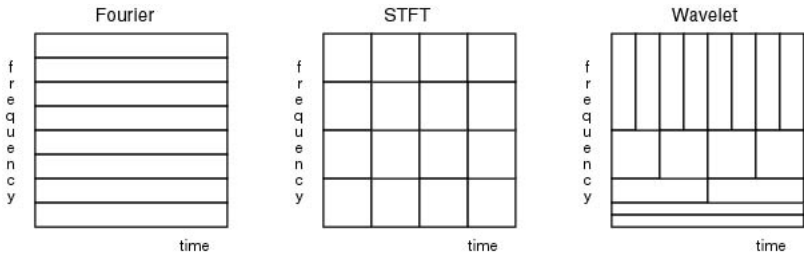

Figure 4. The sampling of the time-frequency plane for different transforms.

Wavelets

Because wavelets are very efficient in representing non-stationary signals and images, it has become an important research area. To analyse a signal with wavelets an elementary function is used. It is called the mother wavelet and is localized both in frequency and in time. The mother wavelet is then scaled and time-shifted and applied to the signal. An important difference between the STFT and the wavelet transform is the sampling of the time-frequency plane. For the STFT the frequency and time resolution is constant, but for the wavelet transform frequency resolution is better for low frequencies than for higher frequencies and vice versa for the time resolution, see Figure 4.

Continuous wavelet transform

For a signal $x(t)$, the continuous wavelet transform (CWT) is expressed as:

$$CWT(a,b) = \int x(t)\psi^{*}_{a,b}(t)dt, \tag{7}$$

where

$$\psi_{a,b}(t) = \frac{1}{\sqrt{|a|}}\psi\left(\frac{t-b}{a}\right) \tag{8}$$

is the scaled and time-shifted mother wavelet. A popular wavelet for calculating CWTs is the Morlet wavelet (Vetterli and Kovačević, 1995), which is defined as:

$$\psi(t) = \frac{1}{\sqrt{2\pi}} e^{-j2\pi f_0 t} e^{-t^2/2}. \tag{9}$$

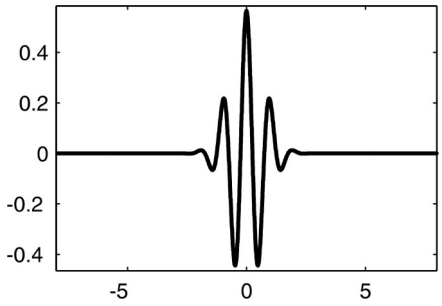

Figure 5. The real part of a Morlet wavelet.

The real part of the Morlet wavelet can be seen in Figure 5. The figure clearly shows that the Morlet wavelet is a Gaussian-shaped sine wave.

If the signal $x(t)$ needs to be reconstructed the mother wavelet must meet the following admissibility condition:

$$C_\psi = \int \frac{|\Psi(f)|^2}{|f|} df < \infty, \tag{10}$$

where $\Psi(f)$ is the Fourier transform of the mother wavelet $\psi(t)$. The signal $x(t)$ can then be reconstructed by:

$$x(t) = \frac{1}{C_\psi} \iint CWT(a,b)\psi_{a,b}(t) \frac{dadb}{a^2}. \tag{11}$$

The CWT is actually a time-scale representation instead of a TFR. For a wavelet localized around the frequency f_0 the frequency can be calculated as $f = f_0 / a$, and the CWT(a,b) can be a function of time and frequency by:

$$CWT(a,b)\big|_{a=\frac{f_0}{f}, b=t} = TFR\left(\frac{f_0}{f}, t\right). \tag{12}$$

An important property of the CWT is that the energy in the time domain is equal to the weighted energy in the time-frequency domain.

$$\int |x(t)|^2 dt = \frac{1}{C_\psi} \iint |CWT(a,b)|^2 \frac{dadb}{a^2}. \tag{13}$$

As in the STFT the squared magnitude of the transform is often used. For

the CWT it is called scalogram. Calculating a true CWT is not possible to do numerically. However, in practice a wavelet transform where a frequency spectrum is calculated for every time sample is considered to be a CWT.

Bilinear distributions

The normalised squared magnitude of the Fourier transform is known as the periodogram or the power spectrum. The power spectrum can also, with help from the Wiener-Khinchin theorem, be expressed as the Fourier transform of the auto-correlation function of the signal. The basic idea for all bilinear distributions is to make the auto-correlation function time-dependent to receive a time-dependent power spectrum. All time-frequency bilinear distributions can be written as (Cohen, 1995):

$$C(f,t) = \iiint x\left(u+\frac{\tau}{2}\right)x^*\left(u-\frac{\tau}{2}\right)\phi(\theta,\tau)e^{-j\theta t - j2\pi f\tau + j\theta u}\,du\,d\tau\,d\theta. \quad (14)$$

The function $\phi(\theta,\tau)$ is called the kernel function and defines the different bilinear distributions. A drawback with all bilinear distributions is that the bilinear representation introduces cross-term interference. An important research area has been to reduce the interference and still keep the important properties of the transform. Some of the important properties are the high resolution, time-shift and frequency modulation invariance, and the energy conservation.

Spectral moments

Spectral changes have been used to monitor manifestations of muscle fatigue (Basmajian and DeLuca, 1985). A common spectral change indicator is the mean frequency (MNF), which is the first spectral moment, but higher order spectral moments have also been considered (Merletti *et al.*, 1995; Karlsson 2000). For non-stationary signals the instantaneous MNF (IMNF) and higher order instantaneous spectral moments (ISM_r) should be used instead.

$$IMNF(t) = \frac{\int_0^\infty f \cdot TFR(f,t)\,df}{\int_0^\infty TFR(f,t)\,df}, \quad (15)$$

$$ISM_r(t) = \frac{\int_0^\infty (f - IMNF(t))^r\, TFR(f,t)\,df}{\int_0^\infty TFR(f,t)\,df}. \quad (16)$$

The spectral moments of order three and four are usually expressed in normalised form and are known as the spectral skewness and spectral kurtosis indices (Merletti *et al.*, 1995).

Component analysis

When new variables are calculated as linear combinations of the original variables, the term *component analysis* is sometimes used. The new variables are chosen to better reflect the data, and in some cases those variables can be used to reduce the dimension of the data. When the aim is to find one or a few linear combinations that are interesting the term *projection pursuit* was introduced by Friedman and Tukey (1974). Projection pursuit uses an index of ”interestingness” that should be maximised (Jones and Sibson, 1987). Although any index could be chosen, it has been argued that the Gaussian distribution, in the context of finding clusters or outliers in the data, is the most uninteresting distribution and therefore the projections obtained with projection pursuit are often highly non-Gaussian (Jones and Sibson, 1987), see Figure 6.

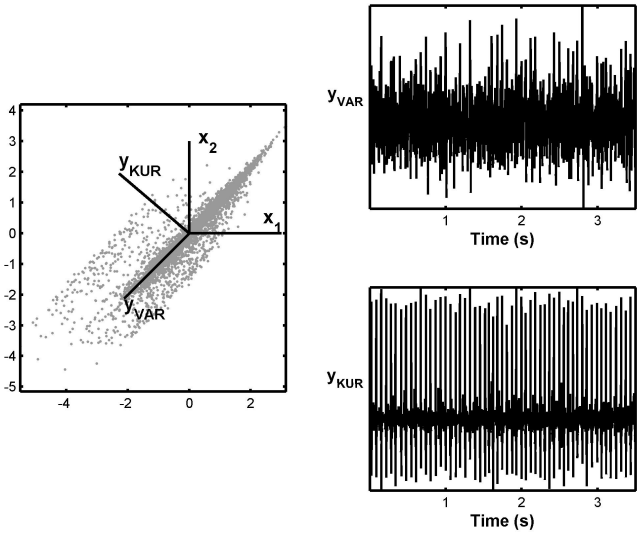

Figure 6. In the left figure the samples of two recorded channels (x_1 och x_2) are plotted. From these channels two linear combinations are computed: y_{VAR}, which is the combination that maximises the variance (first principal component) and y_{KUR}, which is the linear combination that maximises the kurtosis of the output. As seen from the figures on the right the non-gaussian signal y_{KUR} contains the firing instances of an MU.

Principal Component analysis

In principal component analysis (PCA), the new variables are chosen so that the variance of every new variable is maximised with the constraint that it is uncorrelated with the other variables. This procedure gives the possibility to reduce the dimension of the data and still keep as much as possible of the information in a least-square sense. In practice PCA is calculated as eigenvectors of the covariance matrix (the covariance matrix is diagonalised).

Independent Component analysis

In blind source separation (BSS), which is the problem of finding sources by using their mixtures, the independent component analysis (ICA) is now often used. ICA uses the central limit theorem "backwards". The central limit theorem states that the summation of a large number of independent variables tends towards a normally distributed variable regardless of the distribution of the original variables. To find the source signals the "non-gaussianity" is thus maximised. In this context the calculation is very similar to projection pursuit. However, in ICA the number of sources is often known, while projection pursuit is used for exploratory analysis of multivariate data. Maximising the "non-gaussianity" can be achieved in many different ways, for example the joint approximate diagonalisation of eigen-matrices (JADE) algorithm (Cardoso and Souloumiac, 1993) diagonalises fourth-order cumulant matrices and therefore maximises the kurtosis of the new variables. The drawbacks when using JADE for BSS are that it requires much computational power and that kurtosis is too sensitive for outliers. A popular algorithm to perform ICA is the FastICA algorithm (Hyvärinen, 1999), which maximises an approximation of negentropy (using contrast functions). There are also other algorithms, for example MILCA (based on mutual information), Kernel ICA (uses contrast functions), and RADICAL (uses an entropy estimator).

Electromyography techniques

When recording surface EMG it is important to place the electrodes correctly with respect to the innervation zone (IZ). The IZ is the zone that contains the NMJs. Therefore, an easy and reliable method to locate the IZ is needed.

The MNF of the EMG signal is often used as an EMG spectral change indicator and, as such, is used to characterise muscle fatigue. However, the MNF estimate is not reliable when the amplitude of the EMG signal is low.

Techniques for receiving information on single MUs by using

multichannel surface EMG have received great interest in the last few years (Rau and Disselhorst-Klug, 1997a; Roeleveld and Stegeman, 2002; Merletti, Farina and Gazzoni, 2003). The use of surface EMG electrode arrays or grids with small electrodes and small inter-electrode distances, together with spatial filtering techniques (Reucher *et al.,* 1987; Rau and Disselhorst-Klug, 1997a) enables single MUAPs to be obtained. The spatial filter technique is often used in order to limit the number of MUAPs contributing to the surface EMG signal. The traditional filters are *a priori* determined and will therefore have varying effects because the different subjects and different recording situations will markedly affect the characteristics of the recorded surface EMG signal. The MUAP shapes obtained with such high spatial resolution surface EMG are not comparable with MUAP shapes obtained with needle EMG. Nevertheless, rough changes in the surface recorded MUAP are evident for some diseases (Rau *et al.*, 1997b). The high spatial resolution EMG could be used for CV estimation (Farina *et al.*, 2001c; Houtman *et al.*, 2003; Schulte *et al.*, 2003. Grönlund *et al.*, 2005), motor unit characterisation (Roeleveld *et al.*, 1997) and for estimating the firing rate of MUAP trains (Chauvet *et al.*, 2003).

Aims

The general aim of this dissertation was to introduce and evaluate new methods for the analysis of surface EMG signals. The methods were intended to be used in physiological studies, where the variables are compared at group level.

Specific aims

The specific aims were to introduce and evaluate new methods for:

- finding the innervation zone using surface EMG signals (addressed in paper I)
- improved mean frequency estimation of surface EMG signals (addressed in paper II)
- finding single motor unit action potential trains and showing an application of the method by studying the motor unit firing rate of fibromyalgia patients (addressed in papers III, IV and V)

Materials and methods

Although examples of *in vivo* measurements were used, papers I to IV were *in vitro* studies. Paper V was an *in vivo* study.

All EMG signals, except for paper II, were recorded with a modified ActiveOne (Biosemi, Amsterdam, Netherlands) with a 13x10 grid of electrodes with electrode diameter 1.5 mm and with an inter-electrode distance of 5 mm. All data were recorded with a common reference (unipolar recordings), converted from a range of ± 66 mV with 16-bit resolution. The sampling frequency was 2048 Hz and the anti-aliasing filter was a 5th order Bessel filter with -3 dB gain at 512 Hz.

Simulations

To compare different methods in papers I, III and IV, EMG signals were simulated with a slightly modified version of the model presented by Farina and Merletti (2001b). Parameter values were mainly taken from (Farina and Merletti, 2001b) and (Gazzoni *et al.*, 2004). In paper II the Shwedyk model (equation (2)) was used.

Experimental procedures

All papers, except paper V, used simulated data to evaluate the methods. All methodological papers (except paper II) follow the same general outline – simulate data, compare and evaluate different methods, and then show examples using real data. Paper II followed the same outline with the exception that it did not contain any real data.

Subjects

In paper V EMG recordings were obtained from the trapezius muscle from 29 fibromyalgia patiens and 30 controls. In papers I and III EMG recordings from biceps brachii on healthy subjects were used (twelve subjects in paper I and two subjects in paper III). In paper IV EMG signals from a patient who had been exposed to radiation due to cancer were used for showing a possible application of the method. All participating subjects gave their

informed consent before participating in any of the studies.

Location of innervation zone

During recording and in some analyses of surface EMG it is important to know where the IZ is located. Different recommendations on where to place surface EMG electrodes, for example from the SENIAM project (Hermens *et al.*, 1999), are a way to ensure that electrodes are not placed over the IZ. Nevertheless, it would be preferable to know the location of the IZ during multichannel EMG recordings. A technique that is to be used in a recording system must be fast and easy to interpret. The only automatic method available was the lowest root-mean-square (RMS) method (Rainoldi *et al.*, 2004), which used the channel with the lowest RMS as the estimate of the location of the IZ. This technique can be unstable in some cases. Therefore, a modified optical flow technique was used to estimate the location of the IZ. An optical flow field is a vector field that describes the movement between two images. For an introduction to optical flow please see paper II or (Sonka *et al.*, 1998). A multichannel surface EMG can be seen as sampled images describing the potential distribution on the skin. From these images the optical flow fields can be calculated. However, a problem arises because the EMG images do not fulfil the basic assumption in optical flow. This assumption is that the intensities between successive images are not changed but only translated. Because of noise and superposition of APs this assumption is invalid. Therefore the median field during a short time interval is used, see paper I for details.

Estimation of mean frequency

Analysis of the frequency spectra, using the mean frequency, is often used to characterise muscle fatigue. If the frequencies change with time the instantaneous mean frequency (IMNF) is preferable. It can be calculated as:

$$IMNF(t) = \int_{f_L}^{f_H} f \cdot TFR(f,t)df \Bigg/ \int_{f_L}^{f_H} TFR(f,t)df\,, \qquad (17)$$

where f_L is the lowest frequency and f_H is the highest frequency in the bandwidth of the calculated TFR. Especially when the signal-to-noise ratio (SNR) is low the choice of this bandwidth can affect the result. It would be preferable if the integration limits where automatically chosen in an optimal way. A technique to find the maximum frequency of the EMG-spectra and use that frequency as the integration limit was proposed by Knaflitz and Bonato (1999). Knaflitz and Bonato used the threshold crossing

method (TCM) that previously had been used to find the maximum frequency of Doppler signals (D'Alessio, 1985). The TCM was theoretically extended in paper II to include TFRs and gamma distributed frequency bins.

The maximum frequency of the TCM is found when at least r out of m frequency bins exceed a given threshold (starting from the high frequency end of the spectrum). Given the specificity, the threshold can be calculated. When a signal consists of white Gaussian noise with unit variance, the coefficients of a non-negative bilinear TFR are approximately chi-square distributed (Pitton, 2000). Thus, the distribution of the spectral bins can be described with a gamma distribution with the scale parameter λ = ½ and the shape parameter α equal to half the number of degrees of freedom. The threshold of the TCM from a gamma distribution can be calculated as:

$$T_h = G^{-1}\left(1 - P_e \,|\, \alpha, \lambda\right), \tag{18}$$

where P_e can be calculated (given the specificity P_S) from:

$$P_S = 1 - \sum_{j=r}^{m} \binom{m}{j} P_e^{\,j} \left(1 - P_e\right)^{m-j}. \tag{19}$$

G is the cumulative gamma distribution function,

$$G(x|\alpha,\lambda) = \frac{\lambda^{\alpha}}{\Gamma(\alpha)} \int_0^x t^{\alpha-1} e^{-\lambda t}\, dt, \tag{20}$$

where

$$\Gamma(\alpha) = \int_0^{\infty} u^{\alpha-1} e^{-u}\, du. \tag{21}$$

In a TFR the frequency bins are not independent because there is a redundancy in the representation. The problem was solved by using frequency bins located with an offset (that corresponded to the dependency in the representation) from each other. The offset can be calculated from autocorrelations of noise spectra or by calculating the dependency. See (Najmi and Sadowsky, 1997) for an example of how this dependency can be calculated.

A proposed method, the running block threshold method (RBTM) (see paper II), is somewhat similar to the TCM, but uses a sum of n frequency bins in order to set the maximum frequency ($f_{max}(t)$).

$$f_{\max}(t) = \max\left\{ k(t) : \sum_{j=0}^{n-1} TFR\left(k(t) - R \cdot j, t\right) > G^{-1}\left(P_S \,|n\alpha, \lambda\right) \right\} \quad (22)$$

where R is an offset that takes the redundancy of the representation into consideration.

Another existing method to calculate the maximum frequency is the hybrid method. The hybrid method finds the maximum frequency as the intersection between a straight line and the integrated power spectrum (Mo *et al.*, 1988). The line, which starts at the high frequency end of the integrated power spectrum, has a slope that is dependent on the noise power density. For details see paper II.

Adaptive filtration

As mentioned in the introduction section, the term *adaptive filter* in this thesis has a wider meaning then normally used in signal processing literature. Here the term implies that the methods are adapted to the recorded data.

Spatial filtration is a linear combination of signals from different electrodes:

$$\boldsymbol{y} = \sum_i a_i \boldsymbol{x}_i, \quad (23)$$

where a_i is the filter coefficient and $\boldsymbol{x}_i$ is the signal at position i in the filter kernel.

To obtain a filter that adapts to the recorded data and does not use predefined filter coefficients some criteria have to be used for the output function $\boldsymbol{y}$. Since the purpose of the filter is to enhance single MUAP trains it would be desirable to use a criterion which gives clearly visible peaks. One criterion which is sensitive for outliers is the kurtosis of the signal. Therefore this criterion was used in the adaptive filter to enhance MUAP peaks in the output of the filter. The JADE algorithm was used to calculate the output with the maximum kurtosis. An introduction to how the JADE algorithm works can be found in the appendix and in (Cardoso and Souloumiac, 1993; Cardoso, 1999).

If a time filter is introduced along with the spatial filter we can write the filter equation as:

$$\boldsymbol{y} = \sum_i a_i \left(\boldsymbol{h}_i * \boldsymbol{x}_i \right), \tag{24}$$

where $\boldsymbol{h}_i$ is the time filter for the signal at position i in the filter kernel and $*$ stands for convolution. This equation can be rewritten to obtain a linear combination:

$$\begin{aligned} &\boldsymbol{y}[n] = \sum_i a_i \left(\boldsymbol{h}_i * \boldsymbol{x}_i [n] \right) = \\ &\sum_i a_i \sum_m \boldsymbol{h}_i [m] \boldsymbol{x}_i [n-m] \overset{\boldsymbol{w}_i = a_i \boldsymbol{h}_i}{=} \sum_i \sum_m \boldsymbol{w}_i [m] \boldsymbol{x}_i [n-m]. \end{aligned} \tag{25}$$

With this linear combination it is possible to adaptively choose both the spatial and temporal filter coefficients at the same time. If a large multichannel system (larger than the spatial size of the filter) is used, the coefficients can be varied for different positions of the electrode grid, see Figure 7.

The technique for finding the filter coefficients by maximising the kurtosis was used for a spatial filter in paper III and for a spatio-temporal filter in paper IV. In paper V the method in paper IV was used to obtain MU firing rates of fibromyalgia patients and healthy controls.

Note that even if the JADE algorithm is used for the adaptive filter this is not a real ICA application. The theoretical approach is different and in an ICA application the aim is to find independent sources from their linear mixtures by estimating the inverse of the mixing matrix. Different sources in an ICA application are thus found from the spatial information as different linear combinations of the *same* channels. The adaptive filter that was proposed in this dissertation finds different sources by using *different* spatial locations, see Figure 7. Furthermore, the proposed adaptive filter can use both the spatial and the temporal information of the data – ordinary ICA only uses the spatial information.

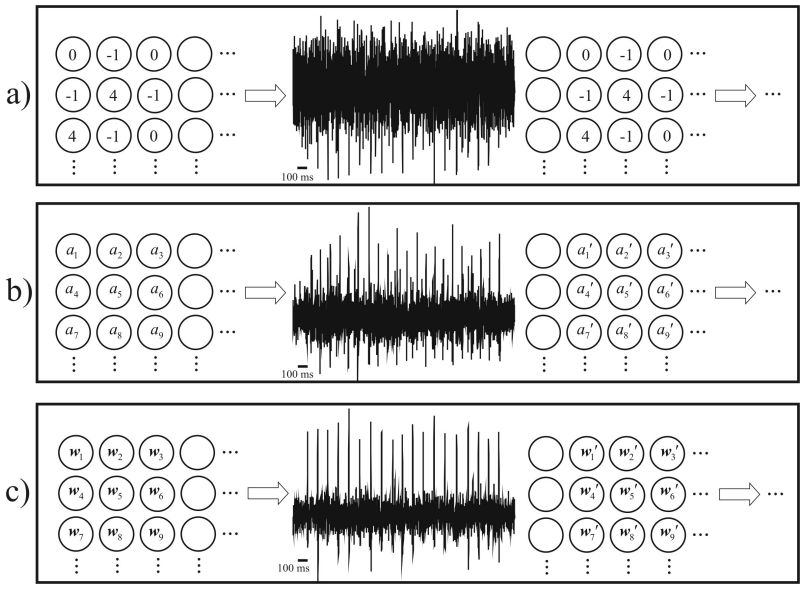

Figure 7. Schematic description of how the filters are applied to a multichannel system. The filter outputs have arbitrary units.
a) At the left the filter coefficients for the NDD filter are shown. The output of this filter when applied to simulated EMG signals is shown in the middle. At the right the new location of the filter would then produce another output and so on.
b) At the left the coefficients (a_1 to a_9) are shown for an adaptive spatial filter calculated in a local neighbourhood. The output of this filter when applied to the same simulated EMG signals as in a) is also shown. At the right the new location of the filter would give new coefficients (a_1' to a_9') that would produce another output and so on.
c) Applying an adaptive spatio-temporal filter (with five time lags) to the same simulated EMG signals as in a) and b) gives the filter output shown. The coefficients ($\boldsymbol{w}_1$ to $\boldsymbol{w}_9$ and $\boldsymbol{w}_1'$ to $\boldsymbol{w}_9'$) are convoluted with the signals.

Spatial and spatio-temporal filters

In paper III the adaptive spatial filter was compared with other spatial filters, and in paper IV the adaptive spatio-temporal filter was compared with other filters that used spatial and/or time information. The spatial filters, for which results were shown in paper IV and in this summary, are the longitudinal single differential (LSD), longitudinal double differential (LDD), normal double differential (NDD), inverse rectangle (IR), and the inverse binomial of order two (IB2) filters. The coefficients for the NDD filter are shown in equation (1) and the other filters' coefficients are shown below:

$$A^{LSD} = \begin{bmatrix} -1 \\ 1 \end{bmatrix}, A^{LDD} = \begin{bmatrix} -1 \\ 2 \\ -1 \end{bmatrix}, A^{IR} = \begin{bmatrix} -1 & -1 & -1 \\ -1 & 8 & -1 \\ -1 & -1 & -1 \end{bmatrix}, A^{IB2} = \begin{bmatrix} -1 & -2 & -1 \\ -2 & 12 & -2 \\ -1 & -2 & -1 \end{bmatrix}.$$

Two methods that used the time information were the weighted low-pass differential (WLPD) filter (Xu and Xiao, 2000) and a method that used the marginal distribution of a CWT from an LDD-filtered signal. The CWT was calculated with a second-order Hermite-Rodriguez function as the mother wavelet (Farina *et al.*, 2000). The definition of the WLPD filter can be seen below:

$$\boldsymbol{y}[n] = \sum_{k=1}^{K} \boldsymbol{v}[k]\left(\boldsymbol{x}[n+k] - \boldsymbol{x}[n-k]\right), \tag{26}$$

where $\boldsymbol{x}$ is an LSD-filtered signal and $\boldsymbol{v}$ is a windowing function of length K.

Results

The four methodological papers (papers I-IV) all introduced methods that had better performance than the existing methods that were included in the comparisons.

Location of innervation zone

Simulations showed that the optical-flow-based method had an error about half the inter-electrode distance, which was 5 mm. The lowest RMS method had about the same magnitude of the errors as long as the SNR was high, see Figure 8.

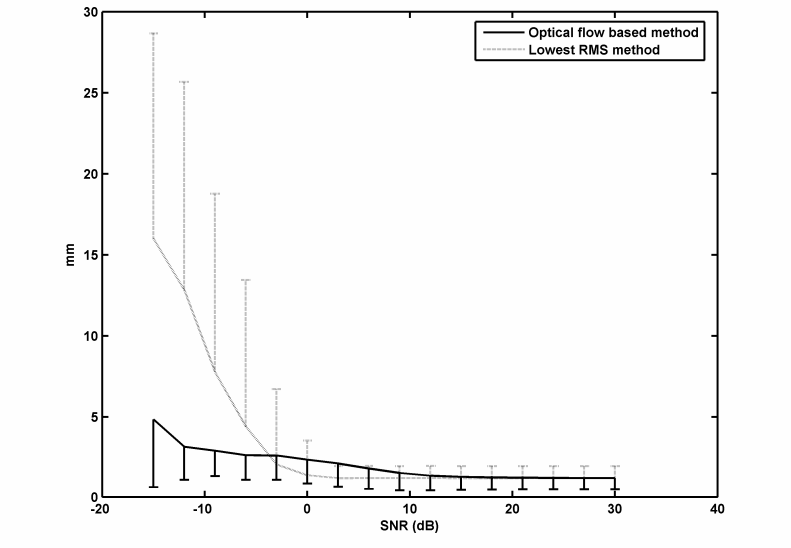

Figure 8. Mean and standard deviation of the absolute localization error of the IZs (from simulations).

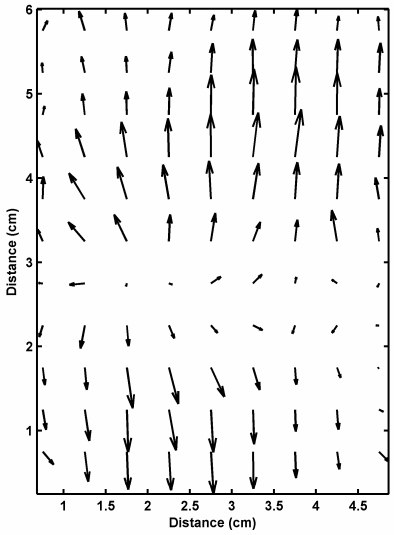

Figure 9. Optical flow obtained from half a second of a multichannel EMG recording, where the electrode device was placed on the biceps brachii. The IZ was approximately located at the position from where the arrows seem to originate.

However, for experimental signals the difference between the methods was larger. On the experimental data the optical-flow-based method gave estimates with absolute errors 2.4 ± 3.4 mm (mean ± standard deviation) as compared with data obtained from an expert group. For the lowest RMS method the absolute errors were 13.6 ± 11.0 mm. In Figure 9 an example of a calculated optical flow field can be seen.

Mean frequency estimation

The detection probability (sensitivity) is defined as the probability of detecting frequency bins that contain information from the signal. This detection probability can be calculated for the proposed method (RBTM) and for the TCM and can be seen in Figure 10. Here it is obvious that the RBTM gave better detection probability for all local SNRs.

The errors for IMNF estimations when different methods were used for finding the integration limit in the IMNF calculations can be seen in Figure 11. See paper II for more detailed results.

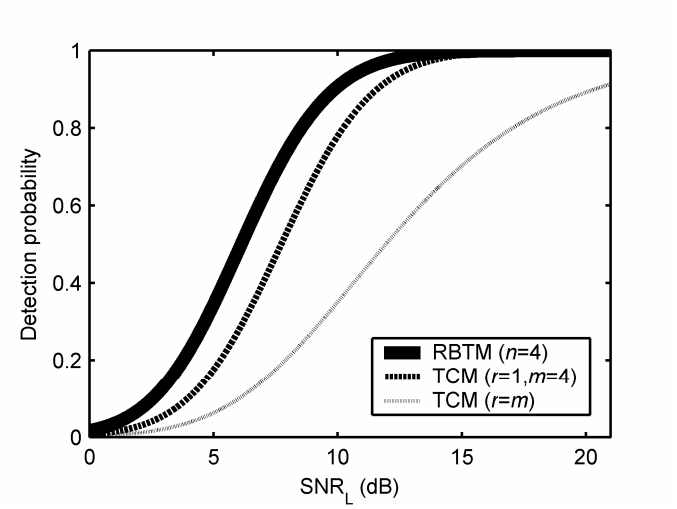

Figure 10. The detection probability at 99.999% specificity for the threshold crossing method (TCM) and the running block threshold method (RBTM) for different local signal-to-noise ratios (SNR$_L$).

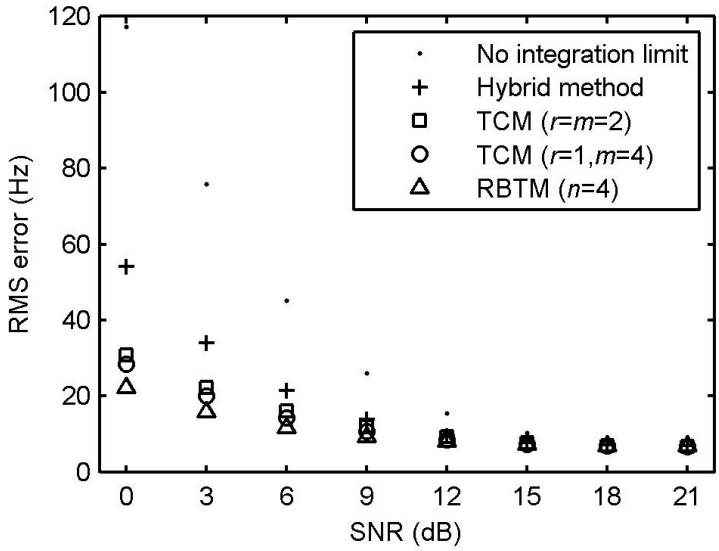

Figure 11. IMNFs from simulated data were calculated using different methods to estimate the maximum frequency. The RMS of the residual error of the estimated IMNF is shown for different SNRs. No integration limit refers to the condition in which the IMNF estimations were calculated on the whole calculated frequency range (up to 700 Hz).

Adaptive filtration

Results obtained with simulated data from the maximum kurtosis filter (MKF) as compared with other filters can be seen in Figure 12. The MKF performed better than the other filters, and both the sensitivity and positive predictivity increased with increasing time length of the filter.

More detailed results can be seen in papers III and IV. The MKF was also used in paper V to obtain single MUAP trains. In that study firing rates obtained from fibromyalgia patients were compared with firing rates from healthy controls, see Figure 13. In paper V results from CV estimations from the fibromyalgia patients and the healthy controls can also be seen.

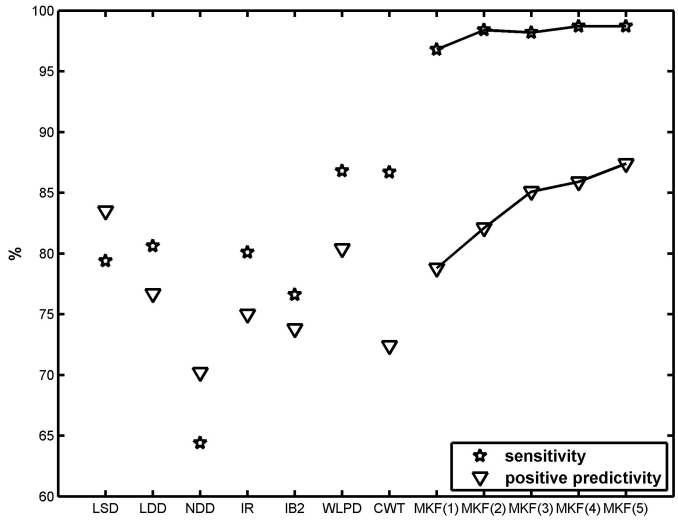

Figure 12. The sensitivity and positive predictivity of different filters. The numbers within the parentheses correspond to the number of time lags in the filter. The results from the MKF filter with different numbers of time lags were connected with a line to visualise the trend.

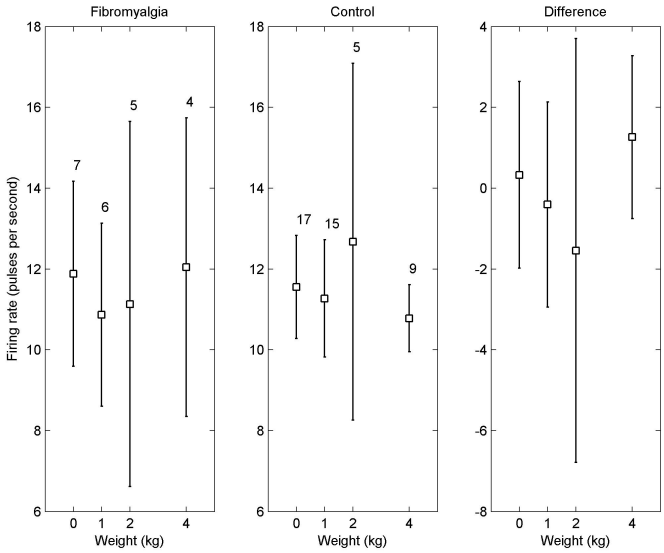

Figure 13. Mean firing rate of MUs (with 95% confidence intervals) of the trapezius muscle for a fibromyalgia group and a control group during isometric shoulder elevation with different loads (weights). The difference between the groups is also shown. The numbers in the graph indicate the number of subjects with valid data and for which the statistics were calculated.

Discussion

This dissertation focused on methods for analysis of surface EMG. The evaluations of the methods are based on simulated EMG signals. The *in vitro* evaluations are necessary because there is no "golden standard" or other easy way to obtain the true answer to the variables that the methods try to obtain. The use of models has a positive side – it is easy to investigate how the methods are affected by different parameters. However, using models also has some negative effects because the models are crude approximations and can never completely mimic a "true" EMG. Furthermore, it is hard to estimate what kind of errors that are introduced in the comparison between methods that are due to the model. Therefore, the absolute numbers obtained in the comparison between different methods must be interpreted carefully. Nevertheless, the order of precedence is not sensitive to errors in the model, and using another model or other parameters would likely result in the same conclusions.

As mentioned in the aim the methods are intended to be used at group level and not to evaluate single subjects. The measured variables have a large physiological variation and the methods only collect information from a part of the muscle. This is especially clear when the firing rate of a single MUAP train is estimated. The MUAP train obtained with the adaptive filter is only one among many possible MUAP trains. If another MUAP train was obtained the estimated firing rate would have been different. Fortunately, at group level, this effect averages out and the distribution of the variables can be compared.

Location of innervation zone

In our opinion, the method that was based on optical flow and was used to obtain the location of the IZ could be interpreted rapidly if the field was visualised with arrows. The method was also easy to automate. Therefore, we believe it would be suitable for use in recording systems for multichannel EMG.

Although we did not specifically attempt to detect muscle fibre orientation, one experimental recording in paper I indicated that this may be another application for the method.

Mean frequency estimation

The calculation of the detection probability is a good way of comparing different methods' abilities to locate the maximum frequency. However, the method that best locates the maximum frequency is not necessarily the best method to use when the integration intervals for IMNF calculations are to be determined. Therefore, the simulations were important. The RMS errors of the IMNF estimates did not only depend on the integration intervals and the noise. The filter implementations and the TFR estimation also introduced errors in the IMNF estimates. Fortunately, those errors were the same for all methods that were compared.

The results showed that it is important to limit the integration interval for IMNF estimates when the SNR is low.

Adaptive filtration

Traditional spatial filters are designed as spatial high-pass filters to enhance the signals located close to the electrodes and to reduce the influence from signals located far from the electrodes. This technique works well under "ideal" conditions. However, since no measuring situation (impedance, volume conductor, etc.) is identical to another, it is not possible to design a fixed spatial filter that works perfectly for all situations. An adaptive filtering technique, although perhaps not necessarily best for every situation, may adjust itself to the recorded signals and may give good results regardless of whether the recording situation is "ideal" or not.

The intent of the introduced adaptive filter was to obtain a signal with clearly visible peaks. Therefore, the kurtosis of the signal was maximised, because a signal with high kurtosis has many small values and a few deviant values.

The filtered signals that are obtained with an adaptive filter have distorted MUAP shapes, but since the firing times of the MUs are detected it is possible to extract MUAP shapes from the monopolar recording by averaging (Disselhorst-Klug *et al.*, 1999; Zwarts and Stegeman, 2003). If the averaging technique is used it is important to ensure that a large majority of the detected firings originate from the same MU. This could be verified by using the MUAP shapes and their amplitude distribution over the skin.

The introduction of the time filtration together with the spatial filtration was a way to increase the information of the signal available to the algorithm. This resulted in a higher sensitivity as well as a higher positive predictivity.

Maximisation of the kurtosis of the signal may not be the best criterion for use in an adaptive filter. It would be interesting to compare different criteria in order to further enhance the performance. A risk with the kurtosis criterion is that it could, in theory, favour MUs with low firing rates. That is because a signal with few firings has a higher kurtosis than a signal with many firings. However, this should be more of a theoretical drawback, since in practice the active MU that is closest to the electrodes is probably chosen.

Using sensitivity and positive predictivity as a measure of performance could be problematic in some cases, because they are to some extent dependent on each other. It would have been preferable to draw an ROC, but this was not possible because the specificity could not be calculated.

Future methods and applications

The experimental signal in paper IV and the study described in paper V showed that it is possible to obtain MUAP trains without using invasive techniques. Paper V also showed that the signal processing methods were only a part of multichannel electromyography. There is still a need for even better and more reliable equipment, collecting procedures, and signal processing methods. Nevertheless, multichannel electromyography today is well suited for many research projects.

I believe surface electromyography would benefit most from new types of electrodes. Unfortunately, developing new types of electrodes is not an easy task. There are, of course, also improvements to be made with signal processing methods. Personally, I think it would be interesting to study different criteria to be used in the adaptive filter that was developed in this dissertation.

The adaptive spatio-temporal technique has been applied to multichannel electrocardiogram (ECG) signals to make a robust heartbeat detector (Ragnarsson *et al.*, 2005). The idea to use this technique to obtain a foetal ECG was also investigated (Östlund *et al.*, 2005). Obtaining the foetal ECG using the spatio-temporal dependence was independently proposed by Stögbauer *et al.* (2004) from the ICA perspective.

Conclusions

This dissertation has resulted in new methods that improve the analysis of EMG signals. As a consequence, the methods can simplify physiological research projects. The innovative methods can inspire other researchers within the EMG field and lead to new and improved methods. The adaptive multichannel filtering technique has resulted in a spin-off effect as a robust heartbeat detector.

Acknowledgements

This dissertation was carried out at the Department of Biomedical Engineering and Informatics at the University Hospital in Umeå. I would like to express my sincere gratitude to those who have helped me with this dissertation. In particular I would like to thank:

Professor Stefan Karlsson, my supervisor, for providing me the opportunity to join the research group, teaching me the methodology of science and introducing me to the EMG field.

Associate Professor Jun Yu, co-supervisor, for taking time to share of his impressive knowledge and for the fruitful discussions.

Professor Björn Gerdle, co-supervisor, for the discussions regarding applications of EMG and for accepting the sometimes tight time schedules.

Professor Ronnie Lundström, head of the Department of Biomedical Engineering and Informatics, for making the research possible.

All the personnel at the research and development department for the stimulating and friendly environment. Especially, I would like to thank co-author Christer Grönlund for the discussions about the methodology of surface EMG.

Associate Professor Karin Roeleveld, co-author, for fruitful discussions and constructive criticism.

The co-authors of papers and proceedings that were not included in this thesis – Andreas Holtermann, Barbro Larsson, Associate Professor Stellan Håkansson, Associate Professor Jack Lind, Per Bergström, Associate Professor Urban Wiklund, Marcus Karlsson, Urban Edström, and Fredrik Ragnarsson.

The Centre for Biomedical Engineering and Physics (CMTF) for providing a forum for discussing biomedical engineering.

My mother and father for their never ending love and support.

Finally, and most importantly, I would like to thank my beloved wife, Hilda, for your love and support in life. I thank my children, Vilhelm and Elsa, for cheering me up and giving me a higher quality of life.

This study was supported with grants from the European Union Regional Development Fund and the Swedish Research Council (K2004-27KX-15053-01A).

References

Adrian E. D. and Bronk D. W. (1929): "The discharge of impulses in motor nerve fibers II: The frequency of discharge in reflex and voluntary contractions", *J. Physiol.*, **67** , pp. 119-151.

Basmajian J. and DeLuca C. J. (1985): *Muscles alive: Their function revealed by electromyography*, 5th ed. (Williams & Wilkins, Baltimore, USA).

Cardoso J.-F. (1999): "High-order contrasts for independent component analysis", *Neural Comput.*, **11**, pp. 157-192.

Cardoso J.-F. and Souloumiac A. (1993): "Blind beamforming for non Gaussian signals", *IEE Proceedings F*, **140**, pp. 362-370.

Chauvet E., Fokapu O., Hogrel J. Y., Gamet D., and Duchêne J. (2003): "Automatic identification of motor unit action potential trains from electromyographic signals using fuzzy techniques", *Med. Biol. Eng. Comput.*, **41**, pp. 646-653.

Clancy E. A., Morin E. L., and Merletti R. (2002): "Sampling, noise-reduction and amplitude estimation issues in surface electromyography", *J. Electromyogr. Kinesiol.*, **12**, pp. 1-16.

Cohen L. (1995): *Time-Frequency Analysis*, (Prentice Hall, Inc., New Jersey, USA).

D'Alessio T. (1985): "'Objective' algorithm for maximum frequency estimation in Doppler spectral analysers", *Med. Biol. Eng. Comput.*, **23**, pp. 63-68.

Darlington R. B. (1970); "Is kurtosis really "peakedness?"", *The American Statistician*, **24**, pp. 19-22.

Disselhorst-Klug C., Rau G., Schmeer A., and Silny J. (1999): "Non-invasive detection of the single motor unit action potential by averaging the spatial potential distribution triggered on a spatially filtered motor unit action potential", *J. Electromyogr. Kinesiol.*, **9**, pp. 67-72.

Farina D., Colombo R., Merletti R., and Olsen H. B. (2001a): "Evaluation of intra-muscular EMG signal decomposition algorithms", *J. Electromyogr. Kinesiol.*, **11**, pp. 175-187.

Farina D., Fortunato E., and Merletti R. (2000): "Noninvasive estimation of motor unit conduction velocity distribution using linear electrode arrays", *IEEE Trans. Biomed. Eng.*, **47**, pp. 380-388.

Farina D. and Merletti R. (2001b): "A novel approach for precise simulation of the EMG signal detected by surface electrodes", *IEEE Trans. Biomed. Eng.*, **48**, pp. 637-646.

Farina D., Mesin L., Martina S., and Merletti R. (2004): "A surface EMG

generation model with multilayer cylindrical description of the volume conductor", *IEEE Trans. Biomed. Eng.*, **51**, pp. 415-426.

Farina D., Muhammad W., Fortunato E., Meste O., Merletti R., and Rix H. (2001c): "Estimation of single motor unit conduction velocity from surface electromyogram signals detected with linear electrode arrays", *Med. Biol. Eng. Comput.*, **39**, pp. 225-236.

Friedman J. H. and Tukey J. W. (1974): "A projection pursuit algorithm for exploratory data analysis", *IEEE Trans. Computers*, **c-23**, pp. 881-890.

Gazzoni M., Farina D., and Merletti R. (2004): "A new method for the extraction and classification of single motor unit action potentials from surface EMG signals", *J. Neurosci. Methods*, **136**, pp. 165-177.

Grönlund, C. (2005): *Muscle fibre characteristics and architecture using multichannel surface electromyograms - A processing methodology*, (Thesis for the degree of licentiate of engineering). Dept. of Radiation Sciences, Umeå University, Sweden.

Grönlund C., Östlund N., Roeleveld K., and Karlsson J. S. (2005): "Simultaneous estimation of muscle fibre conduction velocity and muscle fibre orientation using 2D multichannel surface electromyogram", *Med. Biol. Eng. Comput.*, **43**, pp. 63-70.

Hermens J. H., Freriks B., Merletti R., Stegeman D., Blok J., Rau G., Disselhorst-Klug C., and Hägg G. (1999): *SENIAM 8: European recommendations for surface electromyography*. (Roessingh Research and Development B. V., Enschede, The Netherlands).

Hermens J. H., Hägg G., and Freriks B. (1997): *SENIAM 2: European Applications on Surface Electromyography*. (Roessingh Research and Development B. V., Enschede, The Netherlands).

Houtman C. J., Stegeman D. F., Van Dijk J. P., and Zwarts M. J. (2003): "Changes in muscle fiber conduction velocity indicate recruitment of distinct motor unit populations", *J. Appl. Physiol.*, **95**, pp. 1045-1054.

Huigen E., Peper A., and Grimbergen C. A. (2002): "Investigation into the origin of the noise of surface electrodes", *Med. Biol. Eng. Comput.*, **40**, pp. 332-338.

Hyvärinen A. (1999): "Fast and robust fixed-point algorithms for independent component analysis", *IEEE Trans. Neural Networks*, **10**, pp. 626-634.

Jones M. and Sibson R. (1987): "What is projection pursuit?" *J. Royal Statistical Society*, **150**, pp. 1-36.

Karlsson S., Yu J., and Akay M. (2000): "Time-frequency analysis of myoelectric signals during dynamic contractions: a comparative study", *IEEE Trans. Biomed. Eng.*, **47**, pp. 228-238.

Knaflitz M. and Bonato P. (1999): "Time-frequency methods applied to muscle fatigue assessment during dynamic contractions", *J. Electromyogr. Kinesiol.*, **9**, pp. 337-350.

Lindström L. H. and Magnusson R. I. (1977): "Interpretation of myoelectric power spectra: a model and its applications", *Proc. IEEE*, **65**, pp. 653-662.

Merletti R., Farina D., and Gazzoni M. (2003): "The linear electrode array: a useful tool with many applications", *J. Electromyogr. Kinesiol.*, **13**, pp. 37-47.

Merletti R., Gulisashvili A., and Lo Conte L. R. (1995): "Estimation of shape characteristics of surface muscle signal spectra from time domain data", *IEEE Trans. Biomed. Eng.*, **42**, pp. 769-776.

Merletti R. and Parker P. A. (2004): *Electromyography: Physiology, Engineering, and Noninvasive Applications*. (John Wiley & Sons, Inc., New York, USA).

Mo L. Y., Yun L. C., and Cobbold R. S. (1988): "Comparison of four digital maximum frequency estimators for Doppler ultrasound", *Ultrasound Med. Biol.*, **14**, pp. 355-363.

Najmi A.-H. and Sadowsky J. (1997): "The continuous wavelet transform and variable resolution time-frequency analysis" *John Hopkins APL Technical Digest.*, **18**, pp. 134-140.

Pitton J. W. (2000): "The statistics of time-frequency analysis", *J.Franklin Inst.*, **337**, pp. 379-388.

Ragnarsson F., Östlund N., and Wiklund U. (2005): "Adaptive multichannel filter for heart beat detection", Proceedings of the IFMBE 13th Nordic Baltic Conference on Biological Engineering and Medical Physics, Umeå, Sweden, pp. 299-300.

Rainoldi A., Melchiorri G., and Caruso I. (2004): "A method for positioning electrodes during surface EMG recordings in lower limb muscles", *J. Neurosci. Methods*, **134**, pp. 37-43.

Rau G. and Disselhorst-Klug C. (1997a): "Principles of high-spatial-resolution surface EMG (HSR-EMG): Single motor unit detection and application in the diagnosis of neuromuscular disorders", *J. Electromyogr. Kinesiol.*, 7, pp. 233-239.

Rau G., Disselhorst-Klug C., and Silny J. (1997b): "Noninvasive approach to motor unit characterization: muscle structure, membrane dynamics and neuronal control", *J. Biomech.*, **30**, pp. 441-446.

Reucher H., Rau G., and Silny J. (1987): "Spatial filtering of noninvasive multielectrode EMG: Part I – Introduction to measuring technique and applications", *IEEE Trans. Biomed. Eng.*, **34**, pp. 98-105.

Roeleveld K., Stegeman D. F., Vingerhoets H. M., and Van Oosterom A. (1997): "The motor unit potential distribution over the skin surface and its use in estimating the motor unit location", *Acta Physiol. Scand.*, **161**, pp. 465-472.

Roeleveld K. and Stegeman D. F. (2002): "What do we learn from motor unit action potentials in surface electromyography?", *Muscle Nerve*, **Suppl 11**, pp. S92-S97.

Rosenfalck P. (1969): "Intra- and extracellular potential fields of active nerve and muscle fibres. A physico-mathematical analysis of different models", *Thromb. Diath. Haemorrh. Suppl.*, **321**, pp. 1-168.

Schulte E., Farina D., Rau G., Merletti R. and Disselhorst-Klug C. (2003): "Single motor unit analysis from spatially filtered surface electromyogram signals. Part 2: conduction velocity estimation", *Med. Biol. Eng. Comput.*, **41**, pp. 338-345.

Shwedyk E., Balasubramanian R., and Scott R. N. (1977): "A nonstationary model for the electromyogram", *IEEE Trans. Biomed. Eng.*, **24**, pp. 417-424.

Sonka M., Hlavac V., and Boyle R. (1998): *Image Processing, Analysis, and Machine Vision*, 2nd ed. (Brooks/Cole Publishing Company, Pacific Grove, USA)

Stögbauer H., Kraskov A., Astakhov S. A., and Grassberger P. (2004): "Least-dependent-component analysis based on mutual information", *Phys. Rev. E*, **70,** 066123.

Stulen F. B. and DeLuca C. J. (1981): "Frequency parameters of the myoelectric signal as a measure of muscle conduction velocity", *IEEE Trans. Biomed. Eng.*, **28**, pp. 515-523.

de Talhouet H. and Webster J. G. (1996): "The origin of skin-stretch-caused motion artifacts under electrodes", *Physiol. Meas.*, **17**, pp. 81-93.

Tortora G. J. and Grabowski S. R. (2003): *Principles of Anatomy and Physiology*, 10th ed. (John Wiley & Sons, Inc., New York, USA).

Vetterli M. and Kovačević J. (1995): *Wavelets and Subband Coding*, (Prentice Hall, Inc., New Jersey, USA).

Xu Z. and Xiao S. (2000): "Digital filter design for peak detection of surface EMG", *J. Electromyogr. Kinesiol.*, **10**, pp. 275-281.

Zwarts M. J. and Stegeman D. F. (2003): "Multichannel surface EMG: basic aspects and clinical utility", *Muscle Nerve*, **28**, pp. 1-17.

Östlund N., Wiklund U., Yu J., and Karlsson J. S. (2005): "Adaptive spatio-temporal filtration of bioelectrical signals", Proceedings of the 27th Annual International Conference of the IEEE Engineering in Medicine and Biology Society, Shanghai, China.

Appendix

Introduction to the JADE algorithm

The JADE algorithm are designed to solve an ICA problem, i.e., find the n sources X by using linear mixtures $Y=AX$. The algorithm works in four steps.

- Estimate a whitening matrix W and calculate $Z = WY$ to make the components uncorrelated and of unit variance. This is performed with ordinary PCA.
- Calculate the fourth order cumulants of Z. All second order cumulants can be described by the n x n covariance matrix, but for fourth order cumulants we need n^2 such n x n matrices. If the ICA model holds, only the n most significant cumulant matrices need to be computed.
- Since the data are whitened we can diagonalise the cumulant matrices by computing an orthonormal transformation V. This is performed by a Jacobi technique by minimising the off-diagonals by successive Givens rotations. The rotations are not applied to the data itself but to the calculated cumulant matrices.
- Estimate the sources X by computing V^TZ (^{T} stands for transpose).